J|A|C|S ARTICLES

Published on Web 02/11/2010

Protonated [4*n*]π and [4*n*+2]π Octaphyrins Choose Their Möbius/Hückel Aromatic Topology

Jong Min Lim,[†] Jae-Yoon Shin,[†] Yasuo Tanaka,[‡] Shohei Saito,[‡] Atsuhiro Osuka,*[,‡] and Dongho Kim*[,†]

Spectroscopy Laboratory for Functional π-Electronic Systems and Department of Chemistry, Yonsei University, Seoul 120-749, Korea, and Department of Chemistry, Graduate School of Science, Kyoto University, Sakyo-ku, Kyoto 606-8502, Japan

Received November 17, 2009; E-mail: dongho@yonsei.ac.kr; osuka@kuchem.kyoto-u,ac.jp

Abstract: Protonation-triggered conformational changes of *meso*-octakis(pentafluorophenyl) [36]octaphyrin and [38]octaphyrin have been investigated. The X-ray crystal structures and ^{1}H NMR analyses revealed that the protonation process cuts off intramolecular hydrogen bonds between aminic and iminic pyrrole units and, at the same time, produces intermolecular hydrogen-bond network between aminic pyrrole unit and counter-anions. Such a replacement induces some pyrrole inversion, leading to Möbius aromatic conformation for [36]octaphyrin and to Hückel aromatic conformation for [38]octaphyrin. These protonated octaphyrins show similar structures only with a subtle difference in tilted pyrrole angles, which results in their different topologies. This feature strongly suggests that the macrocycles control their topologies by pyrrole rotation to gain [4*n*]π Möbius or [4*n*+2]π Hückel aromatic stabilization, depending on the number of π-electrons. Detailed photophysical properties such as absorption/fluorescence, excited singlet/triplet state lifetimes, and two-photon absorption cross-section values have been presented for both protonated [36] and [38]octaphyrins in conjunction with their Möbius or Hückel aromaticity.

Introduction

In general, a conformation of an expanded porphyrin depends on various factors, such as structural constraint of macrocycles, a type of substituent, intra/intermolecular hydrogen bond formation, solvent polarity, temperature, and aromaticity/antiaromaticity. These various factors make it difficult to evaluate which one plays a major role in determination of a conformation in respective cases. In this context, it has remained unclear, at least from experimental view, whether aromatic stabilization effect is concerned with the achievement of [4*n*]π Möbius structure of expanded porphyrins.

Recently, [4*n*]π expanded porphyrins have emerged as a promising class of molecules to exhibit [4*n*]π Möbius aromaticity.[1] Apart from the concept of Hückel's aromaticity which is based on the planar structure with [4*n*+2]π electrons, Möbius aromaticity is realized onto the partly distorted and partly planar conformation with [4*n*]π electrons. Since it is hard to get some balance between the degree of distortion and planarity of the molecule, the Möbius aromatic molecules are hardly achieved in usual annulenic systems. Fortunately, distorted Möbius conformations are achieved in expanded porphyrins by their structural diversities to invert or flip out the constituent pyrrole subunits and by overall macrocyclic flexibilities. It was demonstrated that Hückel and Möbius structures coexist as an equilibrium in di-*p*-benzi[28]hexaphyrin(1.1.1.1.1.1),[2] and that fast conformational dynamics among Möbius aromatic conformers and a Hückel conformer occurs in *meso*-aryl substituted [28]hexaphyrin(1.1.1.1.1.1) in solution,[3] where the equilibrium is dependent on solvent and temperature. These reports indicate that there is only a small energy gap between Hückel and Möbius conformations in [28]hexaphyrins. On the other hand, the isolation of rigid Möbius aromatic expanded porphyrins was accomplished by metalation of a series of *meso*-aryl substituted expanded porphyrins, [36]octaphyrin(1.1.1.1.1.1.1.1), [32]heptaphyrin(1.1.1.1.1.1.1), and [28]hexaphyrin(1.1.1.1.1.1).[4] In addition, Rh(I) metalated [24]*N*-fused pentaphyrin(1.1.1.1.1) was assigned as the smallest Möbius aromatic expanded porphyrin.[5] In these metal complexes, their conformations are confined to Möbius structure by metal coordination. Such a metal binding often forces an expanded porphyrin to take a particular conformation regardless of its aromaticity/antiaromaticity.[6] Therefore it cannot be addressed whether aromatic stability leads to the formation of Möbius topology. On the other hand, we have also discovered another method to realize the Möbius aromaticity of expanded porphyrins, intramolecular fusion

[†] Yonsei University.
[‡] Kyoto University.

(1) (a) Herges, R. *Chem. Rev.* **2006**, *106*, 4820. (b) Herges, R. *Nature* **2007**, *450*, 36. (c) Yoon, Z. S.; Osuka, A.; Kim, D. *Nat. Chem.* **2009**, *1*, 113.
(2) Stępień, M.; Latos-Grażyński, L.; Sprutta, N.; Chwalisz, P.; Szterenberg, L. *Angew. Chem., Int. Ed.* **2007**, *46*, 7869.
(3) Sankar, J.; Mori, S.; Saito, S.; Rath, H.; Suzuki, M.; Inokuma, Y.; Shinokubo, H.; Kim, K. S.; Yoon, Z. S.; Shin, J.-Y.; Lim, J. M.; Matsuzaki, Y.; Matsushita, O.; Muranaka, A.; Kobayashi, N.; Kim, D.; Osuka, A. *J. Am. Chem. Soc.* **2008**, *130*, 13568.
(4) Tanaka, Y.; Saito, S.; Mori, S.; Aratani, N.; Shinokubo, H.; Shibata, N.; Higuchi, Y.; Yoon, Z. S.; Kim, K. S.; Noh, S. B.; Park, J. K.; Kim, D.; Osuka, A. *Angew. Chem., Int. Ed.* **2008**, *47*, 681.
(5) Park, J. K.; Yoon, Z. S.; Yoon, M.-C.; Kim, K. S.; Mori, S.; Shin, J.-Y.; Osuka, A.; Kim, D. *J. Am. Chem. Soc.* **2008**, *130*, 1824.
(6) Mori, S.; Osuka, A. *J. Am. Chem. Soc.* **2005**, *127*, 8030.

reactions of *meso*-aryl substituted [28]hexaphyrin(1.1.1.1.1.1).[7] However, such intramolecular bond formations generally take place no matter whether the resulting products are aromatic or not.[8] In this respect, it has remained still difficult to evaluate the relationship between the achievement of Möbius structure and its [4*n*]π aromatic stabilization effect.

In parallel with these reports, we have proved that a protonation method of *meso*-aryl substituted [32]heptaphyrin (1.1.1.1.1.1.1) induces its strong Möbius aromaticity.[9] In this previous report, we showed that intramolecular hydrogen bonds, which are commonly formed between aminic and iminic pyrrole units, are invalidated in acidic conditions. In neutral conditions, the arrangement of such intramolecular hydrogen bonds makes a large difference in the conformation of expanded porphyrins, as well as the number of π-electrons. For example, *meso*-pentafluorophenyl substituted [32]heptaphyrin(1.1.1.1.1.1.1) takes a twisted figure-eight conformation in nonpolar solvents despites its weak [4*n*]π antiaromaticity, because the figure-eight structure makes it possible to form effective intramolecular hydrogen bonds.[8b,9] In acidic conditions, on the contrary, protonated expanded porphyrins are released from the intramolecular binding. Instead, they produce intermolecular hydrogen bonds between aminic pyrrole units and counter-anions (or acid molecules), which often leads to a dramatic transformation in their conformation along with the exhibition of aromaticity. In fact, the above-mentioned [32]heptaphyrins(1.1.1.1.1.1.1) achieve [4*n*]π Möbius structure in acidic conditions, which seems to reflect the aromatic stabilization of [4*n*]π Möbius topology. However, even this result cannot exclude the possibility that the size of heptaphyrin macrocycle is not large enough to take possible Hückel topology without serious constraint and that the Möbius form is relatively stable for the heptaphyrin ligand regardless of its number of π-electrons.

Herein, to elucidate this unsettled but important point, we have compared the protonation effect on a couple of redox congeners, [36] and [38]octaphyrins. To make things clear, we used the octaphyrins which have the same *meso*-aryl substituents in regularly alternating order, namely *meso*-pentafluorophenyl substituted [36]- and [38]octaphyrins(1.1.1.1.1.1.1.1). The differences in these compounds are only the number of π-electrons and the arrangement of intramolecular hydrogen bonds between aminic and iminic pyrrole units. As referred above, intramolecular hydrogen bonds are cut off in acidic conditions. Since the octaphyrin macrocycle is large enough to disregard structural restraint, it is expected that the number of π-electrons plays the most important role in the determination of conformations in acidic conditions. Taking all things into consideration, such large redox congeners in protonated forms are the most suitable case to address the issue on [4*n*+2]/[4*n*] π-electron aromatic stabilization in relation to the topology of expanded porphyrins.

While the structures of expanded porphyrins are unambiguously demonstrated by the X-ray crystal structure analysis, the quantitative evaluation of aromaticity has been continuously pursued especially based on magnetic and π-electron conjugation effects. For instance, diatropic/paratropic ring current in the ^{1}H NMR spectra, NICS (Nucleus-Independent Chemical Shift),[10] BLA (Bond-length Alternation),[11] and HOMA (Harmonic Oscillator Model of Aromaticity)[12] have frequently been used as a quantitative measure of aromaticity. In addition, there have been attempts to explore the structure/property relationship in a comparable set of [4*n*]/[4*n*+2] expanded porphyrins in conjunction with the electronic characters such as UV−visible absorption properties, excited singlet/triplet state lifetimes, and two photon absorption (TPA) cross-section values as a new experimental measure of aromaticity.[13] In this context, the study on the relationship between aromaticity and photophysical properties can provide further insight into the understanding of Hückel/Möbius aromatic molecules.

In this work, the crystal structures of both protonated [36]- and [38]octaphyrins have been successfully determined. Various spectroscopic techniques have been utilized to characterize magnetic and electronic properties in relation to aromaticity, such as ^{1}H NMR titration, spectrophotometric titration, femto- and nanosecond transient absorption and femtosecond Z-scan measurements along with the quantum mechanical calculations.

Experimental Methods

Sample Preparation. *meso*-Octakis(pentafluorophenyl) [36]octaphyrin (1.1.1.1.1.1.1.1) **1** was synthesized according to previously reported method.[14] *meso*-Octakis(pentafluorophenyl) [38]octaphyrin (1.1.1.1.1.1.1.1.1) **2** was quantitatively prepared by the reduction of **1** with $NaBH_4$ in dichloromethane/methanol. In all spectroscopic experiments, dichloromethane was used as solvent (Sigma-Aldrich, spectrophotometric grade) without further purification. Commercial methanesulfonic acid (MSA) and trifluoroacetic acid (TFA) (Sigma-Aldrich, spectrophotometric grade, 99+%) were used as acid for protonation.

X-ray Diffraction Analysis. X-ray data were recorded on a BRUKER-APEX X-ray diffractometer equipped with a large area CCD detector. The structures were solved by Patterson synthesis and refined with the SHELX-97 programs. Single crystals of TFA complex of **1**, which is assigned to diprotonated form of **1** (**1-TFA$_2$**), were obtained from slow crystallization from a mixture of chloroform and heptane solution of **1** in the presence of TFA, while single crystals of TFA complex of **2**, which is assigned to diprotonated form of **2** (**2-TFA$_2$**), were obtained from a mixture of ethyl acetate and isopropyl alcohol solution of **2** in the presence of TFA.

^{1}H NMR Measurement. ^{1}H NMR spectra were recorded on a JEOL ECA-600 spectrometer (600 MHz). Chemical shifts were reported as delta scale in ppm relative to the residual solvent as the internal reference for $\delta = 7.26$ ppm in $CDCl_3$, $\delta = 1.94$ ppm in $CDCN_3$, $\delta = 11.5$ ppm in TFA-*d*. ^{1}H NMR signals were assigned from the ^{1}H−^{1}H COSY spectra and comparison with the spectra

(7) (a) Tokuji, S.; Shin, J.-Y.; Kim, K. S.; Lim, J. M.; Youfu, K.; Saito, S.; Kim, D.; Osuka, A. *J. Am. Chem. Soc.* **2009**, *131*, 7240. (b) Inoue, M.; Kim, K. S.; Suzuki, M.; Lim, J. M.; Shin, J.-Y.; Kim, D.; Osuka, A. *Angew. Chem., Int. Ed.* **2009**, *48*, 6687.
(8) (a) Suzuki, M.; Taniguchi, R.; Osuka, A. *Chem. Commun.* **2004**, 2682. (b) Saito, S.; Osuka, A. *Chem.—Eur. J.* **2006**, *12*, 9095.
(9) Saito, S.; Shin, J.-Y.; Lim, J. M.; Kim, K. S.; Kim, D.; Osuka, A. *Angew. Chem., Int. Ed.* **2008**, *47*, 9657.
(10) (a) Schleyer, P. v. R.; Maerker, C.; Dransfeld, A.; Jiao, H.; Hommes, N. J. R. v. E. *J. Am. Chem. Soc.* **1996**, *117*, 6317. (b) Schleyer, P. v. R.; Chen, Z.; Wannere, C. S.; Corminboeuf, C.; Puchta, R. *Chem. Rev.* **2005**, *105*, 3842. (c) Cyrañski, M. K. *Chem. Rev* **2005**, *105*, 3773.
(11) Schleyer, P. v. R.; Freeman, P.; Jiao, H.; Goldfuss, B. *Angew. Chem. Int., Ed. Engl.* **1995**, *34*, 337.
(12) (a) Kruszewski, J.; Krygowski, T. M. *Tetrahedron Lett.* **1972**, *36*, 3839. (b) Krygowski, T. M. *Chem. Inf. Comput. Sci.* **1993**, *33*, 70.
(13) (a) Yoon, Z. S.; Kwon, J. H.; Yoon, M.-C.; Koh, M. K.; Noh, S. B.; Sessler, J. L.; Lee, J. T.; Seidel, D.; Aguilar, A.; Shimizu, S.; Suzuki, M.; Osuka, A.; Kim, D. *J. Am. Chem. Soc.* **2006**, *128*, 14128. (b) Mori, S.; Kim, K. S.; Yoon, Z. S.; Noh, S. B.; Kim, D.; Osuka, A. *J. Am. Chem. Soc.* **2007**, *129*, 11344. (c) Yoon, Z. S.; Cho, D.-G.; Kim, K. S.; Sessler, J. L.; Kim, D. *J. Am. Chem. Soc.* **2008**, *130*, 6930. (d) Lim, J. M.; Yoon, Z. S.; Shin, J.-Y.; Kim, K. S.; Yoon, M.-C.; Kim, D. *Chem. Commun.* **2009**, 261.
(14) (a) Shin, J.-Y.; Furuta, H.; Yoza, K.; Igarashi, S.; Osuka, A. *J. Am. Chem. Soc.* **2001**, *123*, 7190. (b) Tanaka, Y.; Shin, J.-Y.; Osuka, A. *Eur. J. Org. Chem.* **2008**, 1341.

in the presence of D_2O (signals assigned for NH protons disappear in the presence of D_2O). Since the poor solubility of protonated octaphyrins in $CDCl_3$, the titration experiments were conducted by using $CDCN_3$ solution in which the concentration of octaphyrin is around 10^{-3} M. The solution was titrated with diluted TFA or MSA solution. Variable temperature measurements are performed according to necessity.

UV/Vis/NIR Spectrophotometric Titration. Two milliliters-solution of samples in dichloromethane solvent were titrated carefully in a 1 cm-absorption cell by addition of 0.001, 0.1, 0.5, and 1 M-MSA (or TFA) standard solutions which were made by mixing the acid and dichloromethane with exact ratio of volume. By using a microliter syringe, MSA (or TFA) standard solutions were added in 0.5−10 μL aliquots. After addition of each aliquot, UV/vis/NIR absorption spectra were measured. The total volume change during the titration was corrected by each absorption spectrum multiplied by correction factor, f = (original volume + volume of aliquots)/(original volume).

Steady-State Absorption and Fluorescence Measurements. Steady-state absorption spectra were obtained by using an UV/vis/NIR spectrometer (Varian, Cary5000). For the observation of steady-state fluorescence spectra in NIR region, a photomultiplier tube (Hamamatsu, H9170−75), a lock-in amplifier (EG&G, 5210) combined with a mechanical chopper and a CW He−Cd laser (Melles Griot, Omnichrome 74) for photoexcitation at 442 nm were used.

Femtosecond Transient Absorption Measurements. The femtosecond time-resolved transient absorption (TA) spectrometer consisted of a homemade noncollinear optical parametric amplifier (NOPA) pumped by a Ti:sapphire regenerative amplifier system (Quantronix, Integra-C) operating at 1 kHz repetition rate and an optical detection system. The generated visible NOPA pulses had a pulse width of ∼100 fs and an average power of 1 mW in the range 500−700 nm which were used as pump pulses. White light continuum (WLC) probe pulses were generated using a sapphire window (2 mm of thickness) by focusing of small portion of the fundamental 800 nm pulses which was picked off by a quartz plate before entering to the NOPA. The time delay between pump and probe beams was carefully controlled by making the pump beam travel along a variable optical delay (Newport, ILS250). Intensities of the spectrally dispersed WLC probe pulses are monitored by miniature spectrograph (OceanOptics, USB2000+). To obtain the time-resolved transient absorption difference signal (ΔA) at a specific time, the pump pulses were chopped at 25 Hz and absorption spectra intensities were saved alternately with or without pump pulse. Typically, 6000 pulses excite samples to obtain the TA spectra at a particular delay time. The polarization angle between pump and probe beam was set at the magic angle (54.7°) in order to prevent polarization-dependent signals. Cross-correlation fwhm in pump−probe experiments was less than 200 fs and chirp of WLC probe pulses was measured to be 800 fs in the 400−800 nm region. To minimize chirp, all reflection optics in probe beam path and 2 mm path length of quartz cell were used.

Nanosecond Transient Absorption Measurements. Nanosecond transient absorption spectra were obtained using nanosecond flash photolysis method. The tunable excitation pulse was obtained from an optical parametric oscillator system (Continuum, Surelite OPO) which was pumped by a Nd: YAG laser (Continuum, Surelite II-10). A CW Xe lamp (150 W) was used as a probe light source for the transient absorption measurement. After passing through the sample, the probe light was collimated and then spectrally resolved using a monochromator with a 15 cm f.1. (Acton Research, SP150) equipped with a 600 groove/mm grating. The light signal was detected via an avalanche photodiode (APD) (Hamamatsu, C5331−11). For the temporal profile measurements, the output signal from the APD was recorded using a 500 MHz digital storage oscilloscope (Lecroy, WaveRunner 6050A).

Computational Method. Quantum mechanical calculations were performed with the Gaussian 03 program suite.[15] All calculations were carried out by the density functional theory (DFT) method with Becke's three-parameter hybrid exchange functionals and the Lee−Yang−Parr correlation functional (B3LYP),[16] employing the 6-31G* basis set. In the case of neutral [36]octaphyrin and diprotonated [36]- and [38]octaphyrins, the X-ray crystal structures of **1**, **1-TFA$_2$**, **2-TFA$_2$** were used as initial geometries for geometry optimization without any modification. The NICS values were obtained with the GIAO method at the B3LYP/6-31G* level based on geometry-optimized structures modified by replacing *meso*-substituents with hydrogen atoms. The center of rings for the NICS values was designated at the nonweighted means of π-conjugation pathway of peripheral ring. Moreover other NICS values were also calculated at additional points as the unweighted geometric mean of two interpyrrolic C−N bonds.

Two-Photon Absorption Cross-Section ($\sigma^{(2)}$) Measurements. The TPA measurements were performed using the open-aperture Z-scan method with 130 fs pulses from an optical parametric amplifier (Light Conversion, TOPAS) operating at a 5 kHz repetition rate using a Ti:sapphire regenerative amplifier system (Spectra-Physics, Hurricane X). After passing through a f = 10 cm lens, the laser beam was focused to 1 mm-quartz cell. As the position of the sample cell was varied along the laser-beam direction (z-axis), the transmitted laser beam from the sample cell was then probed using a Ge/PN photodiode (New Focus, 2033) as used for reference monitoring. Assuming a Gaussian beam profile, the nonlinear absorption coefficient β can be obtained by curve fitting to the observed open aperture traces with the following equation:[17]

$$T(z) = 1 - \frac{\beta I_0 (1 - e^{-\alpha_0 l})}{2\alpha_0 (1 + (z/z_0)^2)}$$

where α_0 is a linear absorption coefficient, I_0 is the on-axis peak intensity of the incident pulses at the focal point, l is a sample length, and z_0 is the diffraction length of the incident beam. After obtaining the nonlinear absorption coefficient β, the TPA cross-section $\sigma^{(2)}$ (in unit of 1 GM = 10^{-50} cm^4 s photon^{-1} molecule^{-1}) of a single solute molecule can be determined by using the following relationship:

$$\beta = \frac{\sigma^{(2)} N_A d \times 10^{-3}}{\hbar \nu}$$

Where N_A is the Avogadro constant, d is the concentration of the TPA compound in solution, $\hbar$ is Planck's constant, and υ is the frequency of the incident laser beam. The TPA cross-section value of AF-50 was measured as a reference compound, which was found to exhibit a TPA value of 50 GM at 800 nm.[18]

Results and Discussion

Neutral Species of Octaphyrins. Neutral *meso*-octakis(pentaflourophenyl) [36]octaphyrin(1.1.1.1.1.1.1.1) **1** adopts a doubly twisted figure-of-eight conformation consisting of two porphyrin-like tetrapyrrolic "hemi-macrocycles" as revealed by the previous X-ray diffraction analysis (Chart 1).[14] All pyrrolic nitrogens are pointing inward to form effective intramolecular hydrogen bonds between the aminic and iminic pyrroles. The ^{1}H NMR signals of **1** in $CDCl_3$ for β-protons are located in

(15) Frisch, M. J.; et al. *Gaussian 03*, Revision C.02; Gaussian, Inc.: Wallingford, CT, 2004.
(16) (a) Becke, A. D. *J. Chem. Phys.* **1992**, *98*, 1372. (b) Lee, C.; Yang, W.; Parr, R. G. *Phys. Rev. B.* **1988**, *37*, 785.
(17) Sheik-Bahae, M.; Said, A. A.; Wei, T.-H.; Hagan, D. G.; Van Stryland, E. W. *IEEE J. Quant. Electr.* **1990**, *26*, 760.
(18) Kim, O. K.; Lee, K. S.; Woo, H. Y.; Kim, K. S.; He, G. S.; Swiatkiewicz, J.; Prasad, P. N. *Chem. Mater.* **2000**, *12*, 284.

Chart 1. Molecular Structure of [36]Octaphyrin **1** (left) and [38]Octaphyrin **2** (right)

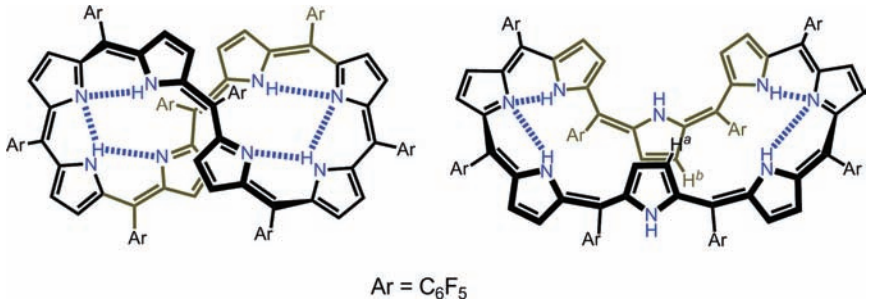

6−8 ppm region and the NICS values are −2.1 to 2.1 ppm at several points around the macrocycle. On the basis of these data, **1** has been regarded as a nonaromatic species.[4] Furthermore, both the crystal structure and DFT optimized structure of **1** revealed distinct bond-length alternation along the conjugated network, in line with its nonaromatic character (Supporting Information, Figure S1). The steady-state absorption spectrum of **1** shows a pair of broad absorption bands at 408 and 637 nm without any Q-like bands in near IR region (Figure 1), which is also a signature of nonaromatic expanded porphyrins.[13]

Although suitable single crystals for X-ray diffraction analysis have not been obtained for neutral *meso*-octakis(pentafluorophenyl) [38]octaphyrin(1.1.1.1.1.1.1.1) **2**, its ^{1}H NMR spectrum in $CDCl_3$ indicates the generation of diatropic ring current by showing β-proton signals in well separated regions of 5.5−7.0 ppm and 2.5−3.0 ppm. Signals observed at 2.51 and 2.78 ppm were assigned to the inner pyrrolic β-protons H^a and H^b and those in a deshielded region to the outer pyrrolic β-protons, hence indicating a diatropic ring current. The moderately shielded signals (δ = 2.51 and 2.78 ppm) suggest that the Hückel conformation is less planar where the protons are not completely lying in the shielding range of the ring current, or

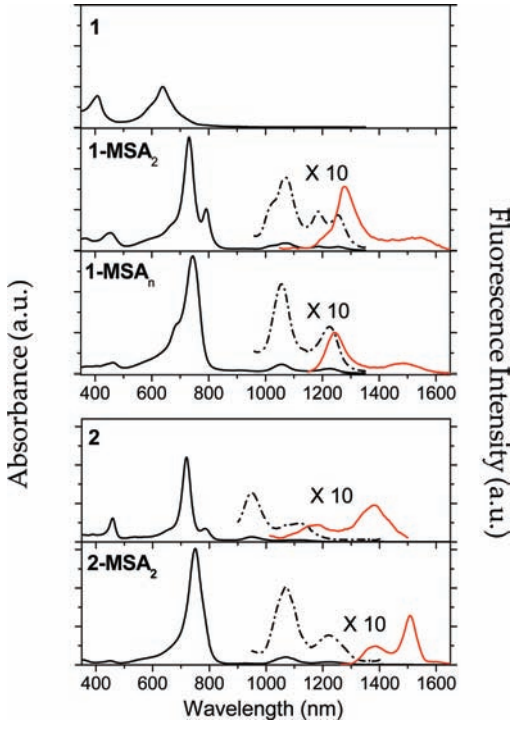

Figure 1. Steady state absorption (black) and fluorescence spectra (red) of [36]octaphyrin **1**, [38]octaphyrin **2**, and their protonated forms (**1-MSA$_2$**, **1-MSA$_n$**, and **2-MSA$_2$**, respectively) upon addition of MSA in CH_2Cl_2.

that there is a dynamic averaging effect among some conformations.[3] Since the low-temperature ^{1}H NMR analysis of neutral [38]octaphyrin **2** in CD_2Cl_2 to 183 K did not show any signal broadening which is the sign of the dynamic equilibrium, the latter possibility was excluded and, at the same time, the sole conformation with relatively low planarity was inferred. In addition, the observed total eight signals for sixteen β-protons indicates some symmetric structure in solution on ^{1}H NMR timescale. The steady-state absorption spectrum of **2** in CH_2Cl_2 shows Soret-like band at 719 nm and Q-like bands at 960 and 1115 nm, which are also characteristic of aromatic expanded porphyrins (Figure 1).[13] These spectral features suggest a 38π-electronic Hückel aromatic conformation with two inverted pyrroles for neutral **2**, as indicated in Chart 1.

Protonated Species of Octaphyrins. X-ray Crystal Structures, ^{1}H NMR, and Steady-State UV/Vis/NIR Absorption Analyses. The X-ray crystal structures of both protonated **1** and **2** were unambiguously revealed.[19] The crystal structure of protonated [36]octaphyrin **1** is shown in Figure 2. Doubly twisted figure-of-eight conformation of neutral **1** was dramatically changed to an extended conformation upon protonation. All the intramolecular hydrogen bonds observed in the neutral form are replaced by intermolecular hydrogen bonds with TFA molecules. Pyrrolic nitrogen atoms at the pyrrole rings **A, C**, **D**, **F**, and **G** point outward to construct the hydrogen bonding network with surrounding TFA molecules. Detailed analysis of the crystal structure led to the assignment of the protonated species to be a dication of [36]octaphyrin **1** (**1-TFA$_2$**).[19] A large and flexible macrocycle of [36]octaphyrin allows its smooth π-conjugation with an overall twisted Möbius topology, in which the torsional angles along the π-conjugation pathway are smoothly settled within 30°.[20]

Aromaticity of protonated [36]octaphyrins was confirmed by ^{1}H NMR measurements that were conducted by controlling temperature and the amount of acids to be added (Supporting Information, Figure S4−S7). The TFA titration NMR spectra

(19) Crystallographic data for **1-TFA$_2$**: $C_{104}H_{28}F_{64}N_8O_{16}$, M_w = 2861.35, monoclinic, space group *C*2/*c* (No.15), a = 30.357(2), b = 22.0294(16), c = 38.924(4) Å, β = 104.353(2)°, V = 25218(4) Å^3, Z = 8, R_1 = 0.0937 [$I > 2.0\sigma(I)$], R_w = 0.2897 (all data), GOF = 1.066 [$I > 2.0\sigma(I)$]. For **2-TFA$_2$**: $C_{116}H_{77}F_{46}N_8O_{15}$, M_w = 2861.35, monoclinic, space group *C*2/*m* (No.12), a = 34.518(5), b = 25.907(4), c = 15.380(2) Å, β = 108.491(3)°, V = 13044(3) Å^3, Z = 4, R_1 = 0.1011 [$I > 2.0\sigma(I)$], R_w = 0.3004 (all data), GOF = 0.962 [$I > 2.0\sigma(I)$]. These values have been obtained by removal of solvent molecules using the PLATON SQUEEZE program. The assignment of diprotonated forms are based on the number of TFA counteranions. The counteranions are distinguished from neutral TFA molecules by the careful analysis of the C−O bond lengths and of the arrangement of hydrogen bonding network. CCDC-753343 (**1-TFA$_2$**) and 753344 (**2-TFA$_2$**) contain the supplementary crystallographic data for this paper.

(20) (a) Rzepa, H. S. *Chem. Rev.* **2005**, *105*, 3697. (b) Heilbronner, E. *Tetrahedron Lett.* **1964**, *5*, 1923.

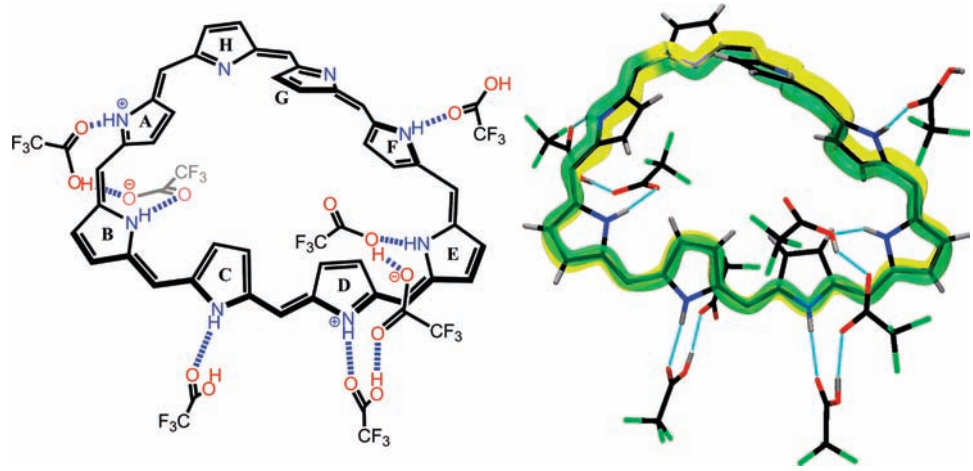

Figure 2. X-ray crystal structure of diprotonated [36]octaphyrin **1-TFA$_2$**. *meso*-Aryl substituents and hydrogen atoms of solvent molecules are omitted for clarity.

in CD_3CN at 233 K showed a gradual decrease in the signal intensities due to neutral octaphyrin **1** followed by a gradual increase in the same signals due to protonated species such as mono- and diprotonated [36]octaphyrin **1-TFA$_1$** and **1-TFA$_2$**. After the addition of three equivalents TFA, the signals of **1** disappeared and the signals of **1-TFA$_1$** and **1-TFA$_2$** were simultaneously observed. These protonated species gave several signals in the region of −1 to −2 ppm and −3 to −5 ppm, respectively, due to the highly shielded inner β-protons, reflecting their substantial aromaticity. Further addition of 10 equiv of TFA led to a simple ^{1}H NMR spectrum consisting of the signals of only **1-TFA$_2$**. Even excess amount of TFA addition or using TFA-*d* solution did not produce any further protonated species such as **1-TFA$_n$** (n = 3 or 4). Thus it can be concluded that [36]octaphyrin **1** is protonated up to dication species by TFA. Then, MSA titration in CD_3CN was examined. The experiments with MSA gave similar spectral changes with the generation of **1-MSA$_1$** and **1-MSA$_2$**, suggesting a mild counteranion effect in the protonation of [36]octaphyrin **1**. The highly shielded inner β-protons show that the aromaticity of these protonated species is strong and the subtle enhancement can be observed in going from **1-MSA$_1$** to **1-MSA$_2$**. Due to the stronger acidity of MSA, neutral [36]octaphyrin **1** almost disappeared after the addition of equivalent MSA. Unlike the case of TFA, four equivalents of MSA led to the appearance of new signals along with those of **1-MSA$_2$**. The new signals are sharp enough for a definite assignment as sixteen pyrrolic β-CH protons at 9.25, 9.03, 8.81, 8.78, 8.26, 7.81, 7.25, 7.22, 6.64, 6.54, 3.81, 3.11, 0.87, 0.15, −0.25, and −0.80 ppm as well as broad pyrrole NH signals at 15.47, 13.36, and 10.83 ppm at room temperature. These signals are probably due to tri- or tetra-protonated [36]octaphyrin **1-MSA$_n$** (n = 3 or 4). The moderate chemical shifts of the shielded inner β-protons suggest relatively weak aromaticity of **1-MSA$_n$** compared with **1-MSA$_1$** and **1-MSA$_2$**.[21]

In the spectrophotometric titration processes of **1** with MSA, the spectral changes show two-step processes (Figure 3a). In the range of [MSA] = 0−2.72 × 10^{-4} M, a dramatic spectral change was observed with the two isosbestic points at 426 and 667 nm. The broadband at 637 nm is red-shifted to 731 nm with increasing intensity while weak and broad bands appear at 1020, 1075, 1185, and 1254 nm. This spectral feature is corresponding to that of typical aromatic porphyrinoids with sharp Soret-like and distinct Q-like bands.[13] Therefore the observed spectral change indicates the appearance of aromaticity upon protonation. By increasing the MSA concentration up to 3.79 × 10^{-3} M, the Soret-like band became more intense at 742 nm and the Q-like bands became a well-defined structure with contracted peaks at 1054 and 1228 nm. Due to the complex protonation process of [36]octaphyrin **1**, it is hard to make a clear distinction among protonated forms. However, the titration data analyzed by Hill plots reveal that two protons are involved in the first-titration step up to the MSA concentrations of 2.72 × 10^{-4} M (Supporting Information, Figure S8).

For a detailed analysis, the spectrophotometric spectra were subjected to the Singular Value Decomposition (SVD) analysis using the SPECFIT/32 program (Spectra Software Associates). This analysis illustrated three linearly independent optical spectra; monoprotonated, diprotonated and tetraprotonated forms, respectively (Supporting Information, Figure S9). While monoprotonated form disappeared below the MSA concentration of 0.6 × 10^{-3} M, di- and tetraprotonated forms existed in a broad concentration ranges of 1.30 × 10^{-4} to 5.8 × 10^{-3} M and 5.8 × 10^{-3} to 0.8 × 10^{-2} M, respectively. In other words, di- and tetraprotonated forms are two major species in the protonation processes with MSA. As a result, the two protonated forms of **1** in spectrophotometric titration up to the MSA concentrations of 2.72 × 10^{-4} and 3.79 × 10^{-3} M can be assigned as diprotonated **1-MSA$_2$** and multiprotonated **1-MSA$_n$**, respectively (Figure 3a).

X-ray crystal structure of protonated [38]octaphyrin **2** is shown in Figure 4.[19] The structure of protonated **2** is surprisingly similar to that of protonated **1** (**1-TFA$_2$**). The octaphyrin macrocycle has crystallographic mirror symmetry with the perpendicular plane to pyrrole rings **A** and **E**. Pyrrolic nitrogens at pyrrole rings **A**, **C**, **D**, **F**, and **G** point outward as those of **1-TFA$_2$**. The octaphyrin macrocycle is surrounded by TFA, isopropyl alcohol, ethanol and water molecules to form intermolecular hydrogen network.[22] The protonated structure is assigned again to dication form of **2** (**2-TFA$_2$**) by confirmation of the number of counter-anions. In spite of the structural

(21) Excess amount of MSA induced unexpected reduction of [36]octaphyrin to [38]octaphyrin. This may be because highly protonated species are susceptible to unexpected reduction due to their positive-charged electron-deficient character.

(22) Ethanol molecule probably comes from the hydrolysis of ethyl acetate which is used as crystallization solvents.

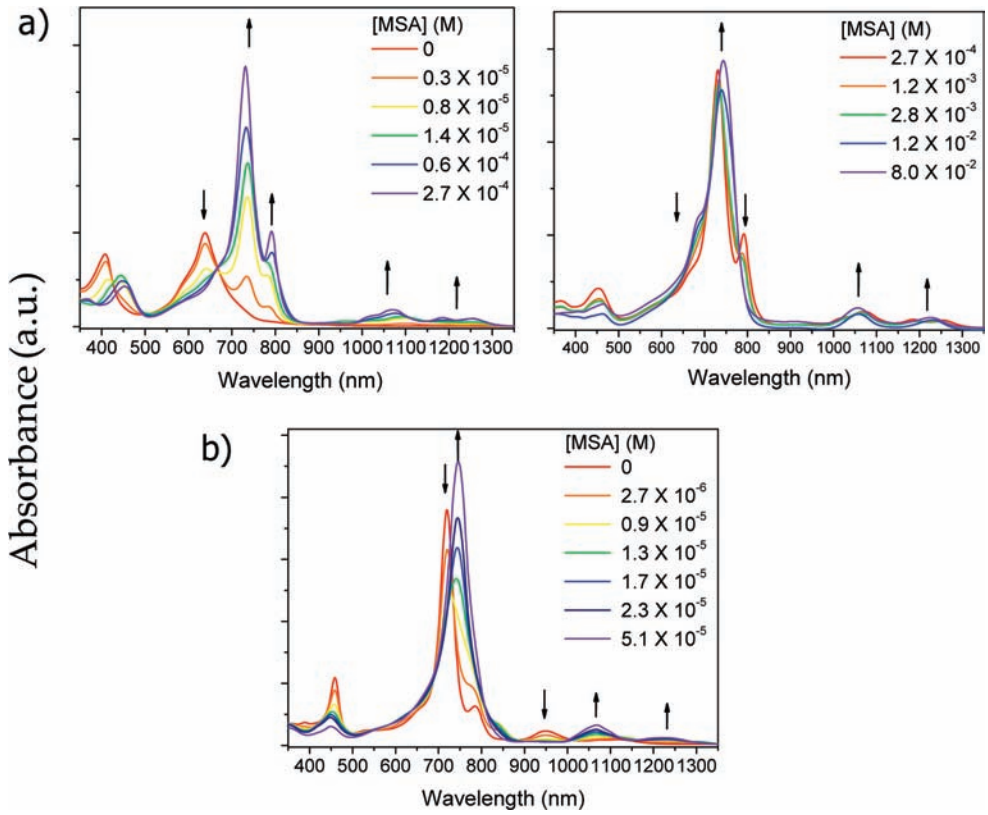

Figure 3. Spectrophotometric titration of (a) **1** and (b) **2** with MSA in CH_2Cl_2.

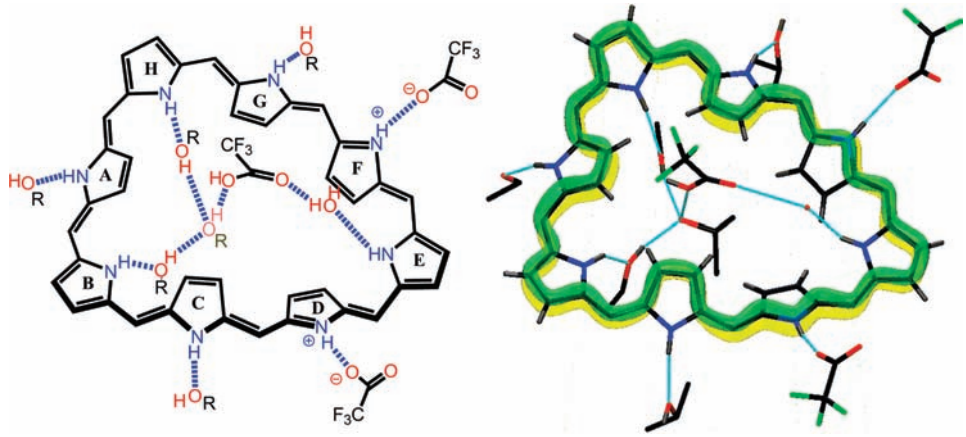

Figure 4. X-ray crystal structure of diprotonated [38]octaphyrin **2-TFA$_2$**. *meso*-Aryl substituents and hydrogen atoms of solvent molecules are omitted for clarity.

similarity to **1-TFA$_2$**, π-conjugation circuit of **2-TFA$_2$** shows double-sided Hückel topology. The distinction of Möbius/Hückel topology between **1-TFA$_2$** and **2-TFA$_2$** originates from the subtle difference in tilt angles at pyrrole **F** and **G**. In the crystal structure of **2-TFA$_2$**, all the pyrrole planes containing **F** and **G** face toward almost the same direction and give rise to approximately planar Hückel conformation, whereas the **F** and **G** rings in **1-TFA$_2$** are significantly tilted to the plane made up of the other pyrrole units and exhibit overall Möbius topology in the crystal structure of **1-TFA$_2$**.[20]

The ^{1}H NMR titration analysis shows simple one-step spectral change from **2** to protonated species by adding TFA or MSA. Although the signals for the protonated form are very broad even at 183 K, it is apparent that this species has a symmetric structure because the number of peaks is small (Supporting Information, Figure S3). Thus the protonated forms may be corresponding to dication species of [38]octaphyrin (**2-TFA$_2$** and **2-MSA$_2$**), whose structure has a mirror symmetry as revealed by X-ray diffraction analysis. Signals for monocation species (**2-TFA$_1$** and **2-MSA$_1$**) were not detected in the titration experiments. The spectrum of **2-MSA$_2$** demonstrates an increased shielding effect upon protonation. The most shielded signal of **2-MSA$_2$** reaches near -10 ppm, while that of neutral [38]octaphyrin **2** is observed only at 2.5 ppm. This large chemical shift in **2-MSA$_2$** probably reflects its more planar conformation upon diprotonation.

The UV/vis/NIR absorption measurement shows almost one-step spectral change upon protonation up to the MSA concentration of 5.14×10^{-5} M with the two isosbestic points at 545 and 1009 nm, although the drastic spectral change was not

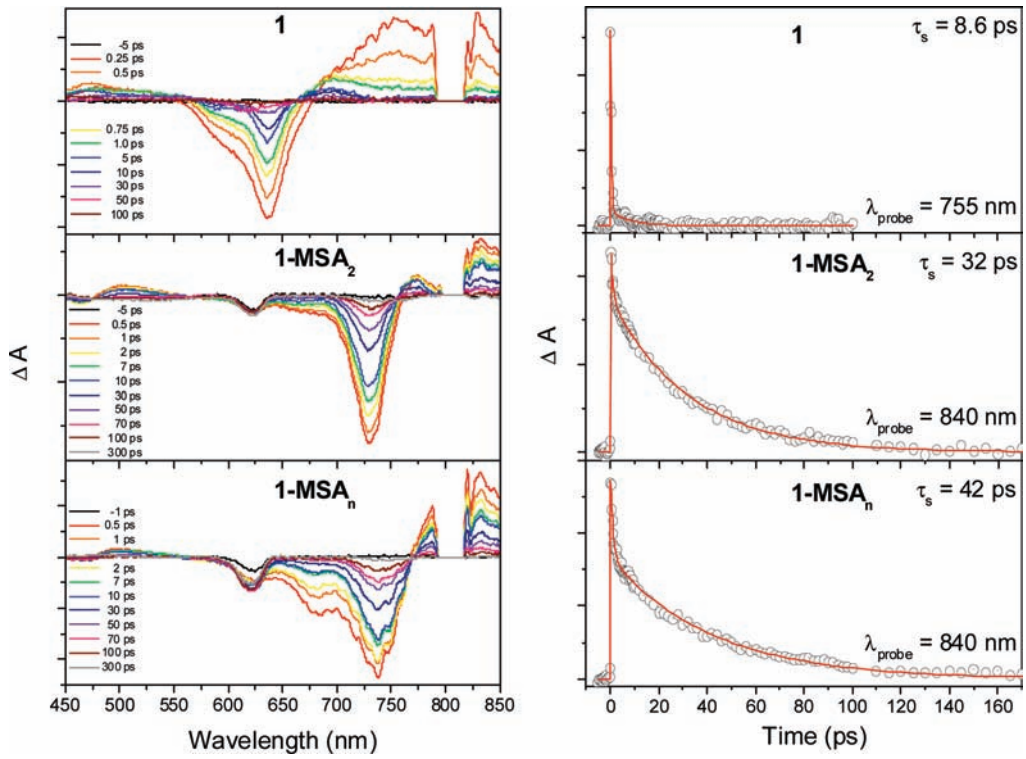

Figure 5. Femtosecond transient absorption decay profiles and spectra of neutral (**1**) and protonated forms (**1-MSA$_2$** and **1-MSA$_n$**) of [36]octaphyrin. For all cases, the pump excitation is at 620 nm.

observed in the protonation process (Figure 3b). Further spectral change was not observed by the addition of MSA. Thus the observed spectrum at [MSA] = 5.14×10^{-5} M is assigned to that of **2-MSA$_2$**. The protonation process is characterized by the intensified Soret- and Q-like bands with bathochromic shifts to 746, 1068, and 1227 nm, respectively. These increased absorption bands correspond to the enhancement of aromaticity in going from **2** to **2-MSA$_2$**, as indicated by ^{1}H NMR analysis.

By considering 36 and 38 π-electron numbers of **1-TFA$_2$** and **2-TFA$_2$**, it is suggested that the protonated octaphyrins favor to take a twisted conformation and a planar conformation, respectively, to realize [4*n*]Möbius and [4*n*+2]Hückel aromaticity to meet the number of π-electrons. Such a facile control of topology means that the octaphyrin macrocycle is large enough to take its preferable topology without serious structural constraint. Under acidic condition, the intramolecular interactions are eliminated, thus rendering the octaphyrin macrocycle to behave according to the number of π-electrons. It also implies that "Möbius aromatic stabilization effect" induces Möbius conformation of protonated [36]octaphyrin,[23] although it is difficult to calculate its numerical energy value. But there still remains a possibility that some particular intermolecular interactions caused by solvent or added acid may determine the predominant conformation not by the number of π-electrons. Such a possibility cannot be completely excluded at the present stage.

Time-Resolved Spectroscopic Analysis. To obtain detailed information on the photophysical properties of expanded porphyrins upon protonation, we have comparatively investigated the excited-state dynamics of neutral and protonated expanded porphyrins.[24] The decay profiles of ground-state bleaching recovery and excited state absorption signals for neutral and protonated [36]octaphyrins in femtosecond transient absorption measurements exhibit complex decay dynamics. We can assign the decay time component of shorter than 1 ps as an energy relaxation processes from higher to lowest excited state such as a relaxation process from S_2 to S_1 state.[25] Since the neutral form of [36]octaphyrin **1** has a structural flexibility, it shows a probe wavelength dependence on the singlet excited state lifetimes of 8.6 ps at 755 nm and 21.5 ps at 640 nm, respectively (Figure 5). This feature may also be attributable to the conformational heterogeneities of [36]octaphyrin **1** in solution. On the other hand, the singlet excited state lifetime of **2** does not show any probe wavelength dependence, 13.7 ps at 720 nm and 12.1 ps at 832 nm (Figure 6). In the nanosecond flash photolysis measurements, neither bleaching nor excited state absorption signal of **1** was detected presumably due to its fast internal conversion process and low intersystem crossing yield as evidenced by fast internal conversion processes of the singlet excited state. On the contrary, we could observe weak triplet excited state absorption and bleaching recovery signals of **2** with the lifetime of 1.38 μs (Supporting Information, Figure S10), supporting that **2** preserves planar Hückel aromatic structure due to its [4*n*+2] π-electron circuit even in its neutral form.

After adding MSA to solution, the excited singlet state lifetimes of **1-MSA$_2$** (32 ps) and **1-MSA$_n$** (42 ps) become definitely longer than that of **1** (Figure 5). The decay profiles of ground state bleaching recovery and excited state absorption signals of **2-MSA$_2$** also exhibit increased decay time constants

(23) (a) Zimmerman, H. E. *J. Am. Chem. Soc.* **1966**, *118*, 6317. (b) Aihara, J.; Horibe, H. *Org. Biomol. Chem.* **2009**, *7*, 1939.

(24) Shin, J.-Y.; Lim, J. M.; Yoon, Z. S.; Kim, K. S.; Yoon, M.-C.; Hiroto, S.; Shinokubo, H.; Osuka, A.; Kim, D. *J. Phys. Chem. B* **2009**, *113*, 5794.

(25) Kang, S.; Hayashi, H.; Umeyama, T.; Matano, Y.; Tkachenko, N. V.; Lemmetyinen, H.; Imahori, H. *Chem. Asian J.* **2008**, *3*, 2065.

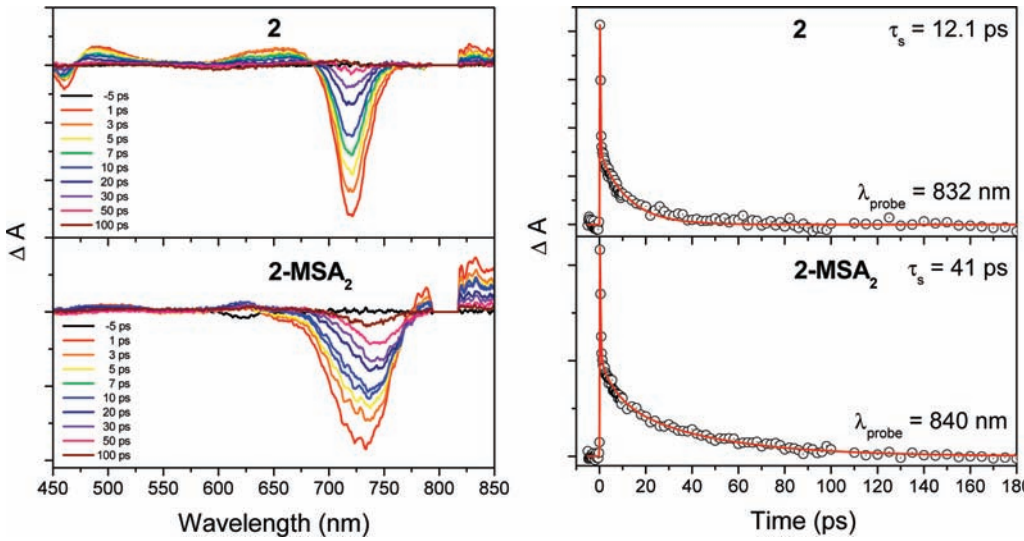

Figure 6. Femtosecond transient absorption decay profiles and spectra of neutral (**2**) and protonated form (**2-MSA$_2$**) of [38]octaphyrin. For all cases, the pump excitation is at 620 nm.

Table 1. Steady-State Absorption and Fluorescence Bands Maxima, Stokes Shifts, Excited Singlet and Triplet State Lifetimes, Two-Photon Absorption Cross-Section $\sigma^{(2)}$, NICS and BLA Values

molecules		λ_{abs} (nm)	λ_{fl} (nm)[d]	ΔE_{Stokes} (cm^{-1})[e]	τ_S (ps)[f]	τ_T (μs)[g]	$\sigma^{(2)}$ (GM) (λ_{ex}/nm)[h]	NICS (ppm)[i]	ΔRx (Å)[k]
[36]octaphyrin	**1**	637[a]	–	–	8.6	–	800 (1280)	−2.1 −2.1[j]	0.126
	1-MSA$_2$	731[a], 791[b], 1250[c]	1275	157	32.1	18.3	5100 (1450)	−9.3[i]	0.083
	1-MSA$_n$	742[a], 1228[c]	1244	105	41.6	0.9, 8.8	2500 (1460)	–	
[38]octaphyrin	**2**	719[a], 1115[c]	1180	494	12.1	1.38	1800 (1420)	–	
	2-MSA$_2$	746[a], 1227[c]	1244	111	40.7	0.22, 2.90	4600 (1420)	−8.8[i]	0.068

[a] Soret-like band. [b] Split B-like band. [c] Lowest energy Q-like band. [d] Fluorescnece band maxima. [e] Energy gap between c and d. [f] Excited singlet state lifetime. Pump and probe wavelength are located in the Supportimg Information, Table S1. [g] Excited triplet state lifetime. [h] λ_{ex} is the excitation wavelength. [i] NICS(0) value at the central position of macrocycle. [j] NICS(0) values at the various positions of macrocycle. [k] Bond length alternation obtained from X-ray crystal structure.

of 50 ps at 730 nm and 41 ps at 840 nm, respectively (Figure 6). Moreover, strong triplet excited state absorption and bleaching recovery signals were observed in **1-MSA$_2$** (18.3 μs), **1-MSA$_n$** (0.9 and 8.8 μs), and **2-MSA$_2$** (0.22 and 2.90 μs) (Supporting Information, Figure S10). Although protonated octaphyrins **1-MSA$_2$** and **1-MSA$_n$** show complicated decay dynamics fitted by two exponential decay components, it is clear that the excited triplet state quantum yield was increased by addition of MSA in solution (Table 1).

Two-Photon Absorption Measurements. We have investigated nonlinear optical properties of **1** and **2** and their protonated forms by using femtosecond Z-scan method to gain further information on the π-electron conjugation.[13,26] To obtain the maximum TPA cross-section values without any contribution from linear absorption, we have scanned the two-photon excitation wavelengths in the wavelength-doubled region of the Soret-like bands for **1** and **2** and their protonated forms (Supporting Information, Figure S11). As a consequence, **1** shows small TPA cross-section value of 800 GM, since the effective π-electron delocalization throughout the whole molecular framework may be hampered by its twisted conformation. As probed by ^{1}H NMR, steady-state and time-resolved spectroscopies, **2** has Hückel aromatic structures, and thus it exhibits relatively larger TPA cross-section value of 1800 GM than **1**. After the addition of MSA to the solutions of **1** and **2**, the TPA cross-section values turn out to be larger than those in neutral conditions, due to the spread and rigid conformation induced by protonation; **1-MSA$_2$** and **2-MSA$_2$** show larger TPA values of ca. 4600−5100 GM than those of their neutral counterparts (Table 1).

Discussion for Photophysical Properties. In our previous studies, a detailed comparative analysis on the photophysical properties of a series of expanded porphyrins was carried out by considering their aromatic characters and conformations.[13] Since the electronic structures of molecules are projected on their photophysical properties, the steady state absorption, excited state dynamics and nonlinear optical properties exhibit distinct features depending on the aromaticity of expanded porphyrins. The porphyrin-like absorption spectra, B- and Q-like bands, are usually observed in aromatic expanded porphyrins with distinct fluorescence spectra. Furthermore, aromatic expanded porphyrins show much longer excited state lifetimes and larger TPA cross-section values than nonaromatic/antiaromatic ones. Not only the experimental results but also the computational calculations such as NICS and BLA values are consistent with the aromatic/antiaromatic nature of expanded porphyrins.[27] Specifically, the photophysical properties of [26] and [28]hexaphyrins illustrate that the excited state dynamics and NLO

(26) (a) Kim, K. S.; Lim, J. M.; Osuka, A.; Kim, D. *J. Photochem. Photobiol. C.* **2008**, *9*, 13. (b) Kwon, J. H.; Ahn, T. K.; Yoon, M.-C.; Kim, D. Y.; Koh, M. K.; Kim, D.; Furuta, H.; Suzuki, M.; Osuka, A. *J. Phys. Chem. B* **2006**, *110*, 11683.

(27) Yoon, Z. S.; Noh, S. B.; Cho, D.-G.; Sessler, J. L.; Kim, D. *Chem. Commun.* **2007**, 2378.

properties are strongly correlated with their geometrical structures and aromatic characters.[28]

Moreover, the aromatic character of expanded porphyrins is controllable with conformational changes by using various methods such as metal-coordination, changing solvent, and addition of acids.[29] For instance, the protonation-triggered conformational changes of expanded porphyrins, *meso*-hexakis(pentafluorophenyl) [30]heptaphyrin(1.1.1.1.1.1.0) and [38]nonaphyrin(1.1.0.1.1.0.1.1.0), gave rise to porphyrin-like symmetric absorption spectra with Soret- and Q-like bands with enhanced aromatic character and increased TPA cross-section values.[24]

The conformational change induced by protonation is not restricted in [4*n*+2] π-electronic systems. The spectrophotometric titrations of **1** show the porphyrin-like symmetric absorption spectra in its protonated forms, **1-MSA$_2$** and **1-MSA$_n$**, suggesting that the twisted structure of [36]octaphyrin **1** is changed to Möbius aromatic structure upon protonation as revealed by X-ray crystallography. On the other hand, the absorption spectra of **2** and its protonated form **2-MSA$_2$** are quite similar, showing that the aromaticity of **2** is preserved upon protonation. Furthermore, the fluorescence behaviors of expanded porphyrins and their protonated forms indicate the conformational differences upon protonation. The reduced Stokes shift of protonated **2** and fluorescence behaviors of protonated **1** indicate the enhancement of structural rigidity upon protonation.

On the basis of the time-resolved spectroscopic results, we can also infer that the molecular flexibility of expanded porphyrins is reduced upon protonation. In general, the nonradiative decay pathways such as internal conversion processes are accelerated in the energy relaxation processes of electronic excited states owing to the molecular flexibility. Therefore, the excited singlet state lifetimes of **1** and **2** indicate that the nonradiative decay channels are stimulated with trembling molecular frameworks;[30] especially, the complex decay components of **1** represent that the relatively variable structure due to its flexible figure-of-eight conformation incites the nonradiative decay processes.[31]

In addition, the enhanced internal conversion process from singlet excited (π,π*) to ground state can cause a decrease of efficiency for the intersystem crossing from singlet to triplet excited (π,π*) state. As a consequence, the molecular flexibility hampers the triplet (π,π*) state formation of **1** by enhancing the internal conversion rate. In this sense, the relatively slow excited singlet/triplet decay of **2** compared with **1** implies the relatively rigid structure imposed by its [4*n*+2] Hückel aromaticity.

On the other hand, the excited state lifetimes of protonated forms become longer than those of the corresponding neutral forms, indicating the enhancement of structural rigidity through conformational change by protonation. While the triplet excited state lifetime of **2** (1.38 μs) is increased by a factor of 2 in its protonated form (2.90 μs), that of **1** becomes drastically longer upon protonation (18.3 μs for **1-MSA$_2$**, 8.8 μs for **1-MSA$_n$**). Overall, the excited state dynamics of expanded porphyrins is strongly correlated with the structural rigidity which is probably affected by its aromatic stabilization effect. In other words, considering the changes in the singlet/triplet excited state lifetimes between neutral and protonated expanded porphyrins, we can suggest that the photophysical properties represent the structural changes with aromatic/nonaromatic character upon protonation.

Nevertheless, for [36]octaphyrin, the fact that the enhancement of aromaticity upon protonation is hard to understand on the basis of Hückel's [4*n*+2] rule. [36]octaphyrin should have antiaromatic character, but the antiaromaticity is interrupted by poor conjugation presumably due to distorted conformation. Instead, upon addition of acids, the distorted conformation of molecules is changed to Möbius structure, where [4*n*]π system can be aromatic. Indeed, the protonated form of [36]octaphyrin **1-MSA$_2$** shows distinct photophysical properties such as symmetric porphyrin-like absorption spectra and increased excited state lifetimes. The excited triplet lifetime of **1-MSA$_2$** (18.3 μs) is longer than those of **1-MSA$_n$** (8.8 μs), **2** (1.38 μs), and **2-MSA$_2$** (2.9 μs). These results indicate that **1-MSA$_2$** shows structural rigidity with its longest triplet excited state lifetime.

Evidently, the enhancement of TPA cross-section value also represents the conformational changes upon protonation. Since the molecular structure is one of crucial factors in the TPA phenomena, third order nonlinear optical property, this process is sensitive to the π-conjugation pathway. In this context, these results indicate that the degree of π-orbital overlap is enhanced along with the conformational change to strongly aromatic structure.

Moreover, when the TPA process occurs near the spectral region of the Soret-like bands, the Q-like bands of expanded porphyrins can play a role of intermediate state in the TPA processes. The enlarged TPA cross-section values of protonated expanded porphyrins (**1-MSA$_2$**, **2-MSA$_2$**) can be interpreted by the bathochromic shift (or appearance) of the Q-like bands. In other words, the enhanced Q-like bands upon protonation act as an intermediate state which induces the enlarged TPA cross-section values.

In particular, the diprotonated form of [36]octaphyrin **1-MSA$_2$** shows the largest TPA cross-section value of 5100 GM which is comparable to those of Hückel aromatic protonated [38]octaphyrin **2-MSA$_2$** (4800 GM) and Möbius aromatic Pd metalated [36]octaphyrin (6400 GM).[4] Thus, we can conclude that the enhanced degree of π-orbital overlap and the appearance of Q-like bands by the Möbius conformation are the important factors in the TPA enlargement of **1-MSA$_2$**.[32] In other words, the largest TPA cross-section value of **1-MSA$_2$** is contributed by the strong aromaticity of smoothly conjugated Möbius conformation.

(28) Ahn, T. K.; Kwon, J. H.; Kim, D. Y.; Cho, D. W.; Jeong, D. H.; Kim, S. K.; Suzuki, M.; Shimizu, S.; Osuka, A.; Kim, D. *J. Am. Chem. Soc.* **2005**, *127*, 12856.

(29) (a) Sessler, J. L.; Morishima, T.; Lynch, V. *Angew. Chem., Int. Ed. Engl.* **1991**, *30*, 977. (b) Chmielewski, P. J.; Latos-Grażyński, L.; Rachlewicz, K. *Chem.—Eur. J.* **1995**, *1*, 68. (c) Lament, B.; Dobkowski, J.; Sessler, J. L.; Weghorn, S. J.; Waluk, J. *Chem.—Eur. J.* **1999**, *5*, 3039. (d) Narayanan, S. J.; Sridevi, B.; Chandrashekar, T. K.; Vij, A.; Roy, R. *J. Am. Chem. Soc.* **1999**, *121*, 9053. (e) Neves, M. G. P. M. S.; Martins, R. M.; Tomé, A. C.; Silvestre, A. J.; Silva, A. M. S.; Félix, V.; Drew, M. G. B.; Cavaleiro, J. A. S. *Chem. Commun.* **1999**, 385. (f) Sessler, J. L.; Seidel, D.; Bucher, C.; Lynch, V. *Chem. Commun.* **2000**, 1473. (g) Sprutta, L.; Latos-Grażyński, L. *Chem.—Eur. J.* **2001**, *23*, 5099. (h) Shimizu, S.; Taniguchi, R.; Osuka, A. *Angew. Chem.* **2005**, *117*, 2265–2269.

(30) Turro, N. J. *Modern Molecular Photochemistry*; The Benjamin/Cumming Publishing Co.: Menlo Park, 1978.

(31) (a) Werner, A.; Michels, M.; Zander, L.; Lex, J.; Vogel, E. *Angew. Chem., Int. Ed.* **1999**, *38*, 3650. (b) Lintuluoto, J. M.; Nakayama, K.; Setsune, J. *Chem. Commun.* **2006**, 3492. (c) Setsune, J.; Tsukajima, A.; Okazaki, N.; Lintuluoto, J. M.; Lintuluoto, M. *Angew. Chem. Int., Ed.* **2009**, *48*, 771. (d) Mori, M.; Okawa, T.; Iizuna, N.; Nakayama, K.; Lintuluoto, J. M.; Setsune, J. *J. Org. Chem.* **2009**, *74*, 3579.

(32) Yoon, M.-C.; Misra, R.; Yoon, Z. S.; Kim, K. S.; Lim, J. M.; Chandrashekar, T. K.; Kim, D. *J. Phys. Chem. B* **2008**, *112*, 6900.

The computational calculations also support the enhanced aromatic character of expanded porphyrins upon protonation (Supporting Information, Figure S12−14). Since the NICS values have been established as a quantitative measure of aromaticity in π-conjugated molecules, we have calculated the NICS values of neutral and protonated expanded porphyrins to support the increase of aromatic character. After geometry optimization using *ab initio* calculation, NICS probe atom Bq (a ghost atom "Banquo") for a molecule was placed in the unweighted geometric center, where the magnitude of magnetic shielding/deshielding induced by π-electronic ring current was calculated. While the NICS values of **1** at various positions were calculated to be in the region of −2.1−2.1 ppm presumably due to its distorted structure and nonaromatic character determined by Hückel's rule,[4] those of diprotonated form based on the optimized geometry from X-ray crystallography of **1-TFA$_2$** obtained large negative values, −9.3 ppm. Thus the NICS values of **1** and its protonated forms are in a good agreement with the fact that the aromaticity of **1-TFA$_2$** increases due to its Möbius conformation.

Since well-defined π-conjugation pathway induces identical bond lengths in macrocycles, the BLA calculations can be another computational method for measuring aromatic character. The BLA value of **1** calculated to be 0.126 Å is reduced to 0.083 Å upon protonation (Table 1). Thus the appearance of aromaticity of protonated expanded porphyrins is accompanied by overall geometric changes upon protonation. As a result, we can conclude that protonated expanded porphyrins, especially **1-TFA$_2$** (or **1-MSA$_2$**) adopts the Möbius topology with a distinct aromatic character.

Conclusions

Protonation effect have been investigated in a couple of redox congeners of expanded porphyrins, pentafluorophenyl substituted [36]- and [38]octaphyrins(1.1.1.1.1.1.1.1) **1** and **2**. X-ray crystal structure, ^{1}H NMR, and steady-state absorption analyses unambiguously determined their protonated structures and aromatic characters. Nonaromatic [36]octaphyrin **1** with figure-of-eight conformation is changed upon protonation to strong Möbius aromatic forms, mono- and diprotonated [36]octaphyrins **1-TFA$_1$** and **1-TFA$_2$** (or **1-MSA$_1$** and **1-MSA$_2$**). The crystal structure of **1-TFA$_2$** revealed that the widely spread conformation is formed with the effective intermolecular hydrogen bonding network. The network made up of the macrocycle, counter-anions and acid molecules replaced the intramolecular hydrogen bonds of the neutral form. On the other hand, weak Hückel aromatic [38]octaphyrin **2** was changed upon protonation to strong Hückel aromatic form, diprotonated [38]octaphyrin **2-TFA$_2$** (or **2-MSA$_2$**). The crystal structure of **2-TFA$_2$** exhibited surprisingly similar conformation to **1-TFA$_2$**, though the Hückel topology of **2-TFA$_2$** is distinct from the Möbius topology of **1-TFA$_2$**. These results strongly suggest that in acidic conditions, in which the macrocycle behaves free from the intramolecular binding, large expanded porphyrins choose their aromatic topology ([4*n*+2]Hückel or [4*n*]Möbius) according to their π-electron numbers to gain aromatic stabilization energy.

We have also investigated the photophysical properties of expanded porphyrins **1** and **2**. In general, as [36]octaphyrin take figure-of-eight nonaromatic conformations due to the flexibilities of molecular frameworks, they revealed (1) no Q-like bands, (2) no fluorescence, (3) short singlet excited (π, π*) state lifetime and low triplet state quantum yield, and (4) low TPA cross-section values. On the contrary, as the protonated forms of **1** and **2** exhibit rigid Möbius/Hückel aromatic structures constructed by intermolecular hydrogen bonding network upon protonation, (1) red-shifted sharp B-like band, (2) Q-like band in NIR region, (3) increased excited state lifetime and (4) enlarged TPA cross-section values became manifest. Based on these results, we could provide an opportunity to find out a simple relationship among structures, excited-state dynamics, and calculated and observed molecular features.

Acknowledgment. The work at Yonsei University was supported by the Star Faculty and World Class University (*R*32-10217) Programs from the Ministry of Education, Science, and Technology (MEST) of Korea and the AFSOR/AOARD Grant (FA2386-09-1-4092). The work at Kyoto University was supported by a Grant-in-Aid (A) (No. 19205006 (A) and 20108001 "pi-Space") for Scientific Research from MEXT. J.M.L. acknowledges the Seoul Science Fellowship and BK 21 Program of the Ministry of Education, Science and Technology. Y.T. and S.S. thank JSPS Research Fellowship for Young Scientists. The quantum calculations were performed using the supercomputing resources of the Korea Institute of Science and Technology Information (KISTI).

Supporting Information Available: Sample preparation, characterization, and X-ray crystallographic details for **1-TFA$_2$** (CCDC-753343) and **2-TFA$_2$** (CCDC-753344). This material is available free of charge via the Internet at http://pubs.acs.org.

JA909744Z